CAMBRIDGE
UNIVERSITY PRESS

RESEARCH ARTICLE

An asymmetric S-curve trajectory planning based on an improved jerk profile

Chol Jun Han[1] (iD), Kwang Rim Song[2] and Un-Ryong Rim[3]

[1]Robotics Institute, Kim Chaek University of Technology, Pyongyang, Democratic People's Republic of Korea
[2]Faculty of Automatics, Kim Chaek University of Technology, Pyongyang, Democratic People's Republic of Korea
[3]Institute of Ocean Engineering, Kim Chaek University of Technology, Pyongyang, Democratic People's Republic of Korea
Corresponding author: Chol Jun Han; Email: hcj901128@star-co.net.kp

Abstract

In this paper, a method of planning the expanded S-curve trajectory of robotic manipulators is proposed to minimize the execution time as well as to achieve the smoother trajectory generation in the deceleration stage for point-to-point motions. An asymmetric parameter is added to the piecewise sigmoid function for an improved jerk profile. This asymmetric profile is continuous and infinitely differentiable. Based on this profile, two analytical algorithms are presented. One is applied to determine the suitable time intervals of trajectory satisfying the time optimality under the kinematic constraints, and the other is to determine the asymmetric parameter generating the minimum execution time. Also, the calculation procedure for the time-scaled synchronization for all joints is given to decrease unnecessary loads onto the actuators. The velocity, acceleration, jerk and snap (the derivative of jerk) of the joints and the end-effector are equal to zero at two end points of motion. The simulation results through 3 DOF and 6 DOF robotic manipulators show that our approach reduces the jerk and snap of the deceleration stage effectively while decreasing the total execution time. Also, the analysis for a single DOF mass-spring-damper system indicates that the residual vibration could be reduced to 10% more than the benchmark techniques in case velocity, acceleration and jerk are limited to 1.24 m/s, 6 m/s^2 and 80 m/s^3, respectively and displacement is set to 0.8m. These results manifest that the performance of reducing residual vibrations is good and demonstrate an important characteristic of the proposed profile suitable for point-to-point motion.

1. Introduction

In recent years, more and more industrial robots have been applied to modern manufacturing systems. They are now fast and smooth with increased precision. However, in order to ensure high productivity and quality, they should be devised even more precisely. For this, trajectory planning for industrial robots is aimed to generate a desired smooth motion with high speed and precision under kinematical and geometrical constraints. In particular, smoothness in motion is essentially required in the delicate industrial setting such as spot-welding or precise assembly, where it is important that the planned trajectories should be continuous within the capability of actuators [1, 2]. Also, the residual vibration is an important issue for high-speed and precise motions [3, 4]. A method based on jerk constraints was efficient for smooth trajectory planning, providing an indirect means to restrict the variation rate of the actuator torques [5]. Jerk constraints are especially significant in reducing machine abrasion, position error and residual vibration [6, 7]. The snap as the derivative of jerk is also the important factor in controlling the trade-off between efficiency and smoothness [8]. The higher snap constraints result in a shorter execution time, while the smoothness is decreased. In contrast with this, the smaller snap constraints result in a longer execution time, while the smoothness is increased. Therefore, the jerk and

snap constraints have to be reasonably chosen in due consideration of the state of the machinery, product precision, productivity and so on.

The planning methods with high-order polynomial are being used for the smooth jerk-limited trajectory planning. Acceleration profiles with high-order polynomial under velocity, acceleration and jerk limits were used for the trajectory planning of several mechanisms [9, 10]. Cubic NURBS curves were extensively used to define the trajectory [11, 12]. Huang et al. improved the smoothness of trajectory planning of robotic manipulator by using the 5th order B-spline [13]. The third-order spline in the Cartesian space was combined with the septuple B-spline in the joint space to generate time-optimal and jerk-continuous trajectories [14]. The time-optimal Acc/Dec method for multiple segments was applied to five-axis machining in ref. [15], where a quintic B-spline corner smoothing method was utilized to smoothen sharp corners in the toolpath. Boryga et al. proposed the planning method of trajectory motions for the 6 DOF manipulator, in which the acceleration profile with higher-order polynomial was determined by one coefficient [16]. Yue et al. achieved the point-to-point trajectory planning of flexible redundant robotic manipulators by using the quadrinomial and quantic polynomials [17]. Wang et al. planned a near time-optimal trajectory by the fourth-order polynomial with the property of root multiplicity, in which the polynomial curve was determined by only one coefficient [18]. Lee et al. proposed an optimization process for polynomial-function-based motion profiles to achieve fast movement with low vibration, where the higher-order continuous trajectory was realized by increasing the degree of the polynomial model [19]. Generally, all the displacement, velocity, acceleration, jerk trajectories made by higher-order polynomial or spline were continuous, but many coefficients should be determined to generate trajectories.

S-curve trajectory planning is widely introduced for generating jerk-constrained motions. An S-curve model ensures reduction of residual vibration and impulse and the smoothness of the trajectory by determining time periods reasonably. Biagiotti et al. presented a new optimization algorithm that assures the minimum possible duration of generalized S-curve trajectories compliant with kinematic limitations and capable of suppressing residual vibrations [20]. Jose et al. developed an S-curve velocity profile which presents an acceleration and deceleration stage smoother than the trapezoidal velocity profile [21]. Ni et al. proposed a novel bidirectional adaptive feedrate scheduling method based on S-shaped acceleration/deceleration algorithm [22]. The third-order polynomial S-curve trajectories for point-to-point motions were proposed, which became one of the widely used models [23, 24]. Hassan et al. generated time-optimal pick-and-throw S-curve trajectories, which was based on a third-order polynomial model [25]. The fourth-order polynomial S-curve model was proposed to eliminate the effect of harmful jerk such as impulse and residual vibration [26, 27]. Li et al. proposed the S-curve trajectory for which Acc/Dec profile was derived from the sinusoidal jerk function [28]. Also, Fang et al. proposed a methodology to generate online smooth joint trajectories of robots based on an improved sinusoidal jerk model [29]. Perumaal et al. generated the trigonometric S-curve trajectory with jerk constraint for the 6 DOF manipulator [30]. Fang et al. proposed the smooth and time-optimal trajectory planning, in which the piecewise sigmoid function was used for generating the jerk profile [8]. A symmetric S-curve trajectory has symmetric acceleration and deceleration stages. Therefore, the smaller jerk and the longer travelling time are needed to reduce the residual vibration effectively in the deceleration stage as well as in the acceleration stage. Therefore, the longer travelling time is needed to generate the smoother motion profile. To meet the requirement of the moving distance and travelling time simultaneously, the asymmetric profile was adopted [31, 32].

Recently, asymmetric trajectories have been presented in several papers to reduce the residual vibration and the settling time. In the asymmetric model, the requirements such as the time optimality and the reduction of the residual vibration can be achieved by making trajectories more aggressive in the acceleration stage and smoother in the deceleration stage. Bai et al. proposed a method for planning an asymmetric *S*-curve trajectory to reduce the residual vibration [33]. Li et al. proposed the time-optimal general asymmetric *S*-curve profile, which was capable of reducing the residual vibration more significantly than the traditional symmetric *S*-curve [34]. The asymmetric S-curve trajectory derived from the
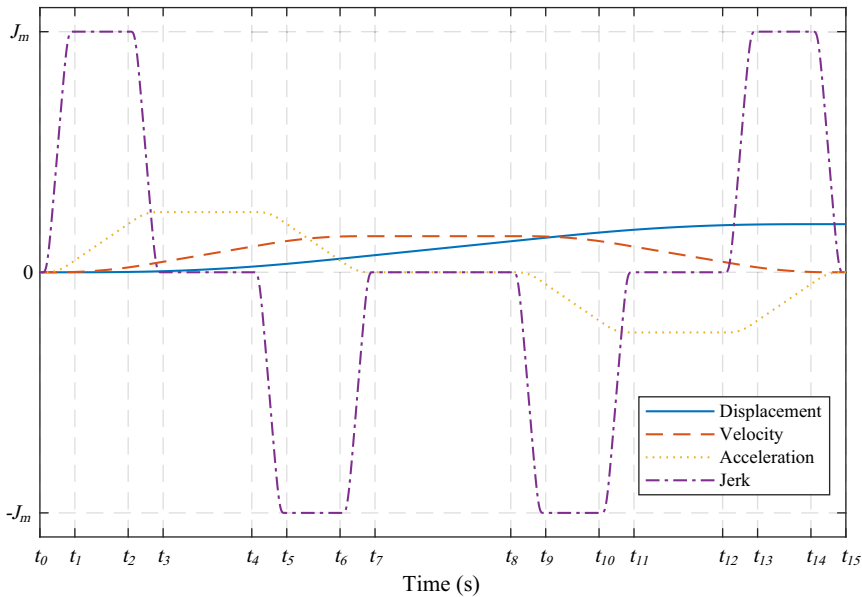
Figure 1. *Kinematic profiles for the normal case of piecewise sigmoid S-curve model [8].*

trigonometric jerk function was presented [35]. Xin and Le proposed a method for planning an asymmetric *S*-type model using the dichotomy iteration and demonstrated that the asymmetric curve had considerable advantages over the symmetric *S*-curve model [36]. Wu et al. improved the motion efficiency of industrial robots using a point-to-point trajectory planning based on a locally asymmetrical jerk profile, where the jerk motion profile was derived from the sinus function [37]. Liu et al. presented the method planning the time-optimal asymmetric *S*-curve trajectory of redundant manipulators under kinematic constraints to design an end-effector motion profile along a specified path [38]. Most asymmetric models are based on the conventional symmetric S-curve profile [34, 39].

In this paper, the symmetric S-curve model proposed in ref. [8] is expanded to an asymmetric one, which will make it possible to minimize the execution time as well as to achieve the smoother trajectory generation in the deceleration stage by decreasing the jerk in the deceleration stage and selecting the asymmetric parameter properly. The aim of this research is to develop a method of planning a new asymmetric S-curve trajectory for improving the smoothness and effectiveness of the motion. To do this, we generate a new asymmetric jerk profile by introducing an asymmetric parameter in the piecewise sigmoid function in the deceleration stage. Then, two analytic algorithms are presented, where one is to decide the time intervals of trajectory satisfying the time optimality under the kinematic constraints and the other is to select the asymmetric parameter for achieving the minimum execution time of motion.

The rest of this paper is presented as follows: Section 2 gives a trajectory planning method based on the improved jerk profile. The simulations of the 3 DOF and 6 DOF robotic manipulators are given in Section 3. The conclusion is drawn in Section 4.

2. Asymmetric S-Curve Trajectory Planning

2.1. Improved jerk profile model

A symmetric jerk profile was proposed by Fang et al. to reduce the complexity of calculation caused by the conventional high-order polynomial models and achieve more effective smoothness than trigonometric models [8]. Fig. 1 shows the kinematic profiles for the normal case of the model proposed in ref. [8].

The jerk profile was defined as follows:

$$
j(t) = sign(D) \cdot
\begin{cases}
J_m \frac{1}{1+e^{-\xi(1/(1-\beta_i)-1/\beta_i)}} & t_0 \leq t < t_1,\ t_{12} \leq t < t_{13} \\[2mm]
J_m & t_1 \leq t < t_2,\ t_{13} \leq t < t_{14} \\[2mm]
J_m \frac{1}{1+e^{\xi(1/(1-\beta_i)-1/\beta_i)}} & t_2 \leq t < t_3,\ t_{14} \leq t < t_{15} \\[2mm]
0 & t_3 \leq t < t_4,\ t_7 \leq t < t_8,\ t_{11} \leq t < t_{12} \\[2mm]
-J_m \frac{1}{1+e^{-\xi(1/(1-\beta_i)-1/\beta_i)}} & t_4 \leq t < t_5,\ t_8 \leq t < t_9 \\[2mm]
-J_m & t_5 \leq t < t_6,\ t_9 \leq t < t_{10} \\[2mm]
-J_m \frac{1}{1+e^{\xi(1/(1-\beta_i)-1/\beta_i)}} & t_6 \leq t < t_7,\ t_{10} \leq t < t_{11}
\end{cases}
\tag{1}
$$

where t_i $(i = 0, 1, 2, \cdots, 15)$ is the initial time instant of the corresponding segment; $\beta_i = (t - t_{i-1})/(t_i - t_{i-1})(i = 1, 3, 5, \cdots, 15)$ is the normalized variable in time period of $[t_{i-1}, t_i]$; ξ is the positive constant corresponding to the variation rate and D is the relative displacement from the initial position that can be either positive or negative.

As shown in Fig. 1, the kinematic profiles for velocity, acceleration and jerk in the acceleration and deceleration stages exhibit the symmetry for the point-to-point motion. They are continuous and infinitely differentiable under the kinematic constraints. For point-to-point trajectory planning, it is important to effectively reduce the residual vibration in the vicinity of the target point in the minimum execution time. To this end, the trajectories in the acceleration stage can be more aggressive, while those in the deceleration stage can be smoother. From this point of view, we expanded the symmetric jerk profile in ref. [8] to an asymmetric profile. The asymmetric jerk profile is defined as follows:

$$
j(t) = sign(D) \cdot
\begin{cases}
J_m \frac{1}{1+e^{-\xi(1/(1-\beta_1)-1/\beta_1)}} & t_0 \leq t < t_1 \\[2mm]
J_m & t_1 \leq t < t_2 \\[2mm]
J_m \frac{1}{1+e^{\xi(1/(1-\beta_3)-1/\beta_3)}} & t_2 \leq t < t_3 \\[2mm]
0 & t_3 \leq t < t_4 \\[2mm]
-J_m \frac{1}{1+e^{-\xi(1/(1-\beta_5)-1/\beta_5)}} & t_4 \leq t < t_5 \\[2mm]
-J_m & t_5 \leq t < t_6 \\[2mm]
-J_m \frac{1}{1+e^{\xi(1/(1-\beta_7)-1/\beta_7)}} & t_6 \leq t < t_7 \\[2mm]
0 & t_7 \leq t < t_8 \\[2mm]
-J_m \frac{\lambda}{1+e^{-\xi\left(1/\left(1-\beta_9\right)-1/\beta_9\right)}} & t_8 \leq t < t_9 \\[2mm]
-\lambda J_m & t_9 \leq t < t_{10} \\[2mm]
-J_m \frac{\lambda}{1+e^{\xi(1/(1-\beta_{11})-1/\beta_{11})}} & t_{10} \leq t < t_{11} \\[2mm]
0 & t_{11} \leq t < t_{12} \\[2mm]
J_m \frac{\lambda}{1+e^{-\xi(1/(1-\beta_{13})-1/\beta_{13})}} & t_{12} \leq t < t_{13} \\[2mm]
\lambda J_m & t_{13} \leq t < t_{14} \\[2mm]
J_m \frac{\lambda}{1+e^{\xi(1/(1-\beta_{15})-1/\beta_{15})}} & t_{14} \leq t < t_{15}
\end{cases}
\tag{2}
$$

where J_m is the maximum jerk in the acceleration stage; λ is the asymmetric parameter $(0 < \lambda \leq 1)$; ξ is the positive coefficient; and $\beta_i = (t - t_{i-1})/(t_i - t_{i-1})$. The kinematic profiles for the normal case are illustrated in Fig. 2, where V_m, A_m and J_m denote the maximum allowable velocity, acceleration and jerk, respectively.

Eq. (2) allows the jerk to vary smoothly between 0 and the maximum allowable value so that the generated trajectories can be infinitely differentiable. The trajectory consists of fifteen segments, whose time interval is denoted as $I_i = t_i - t_{i-1}(i = 1, 2, \cdots, 15)$.
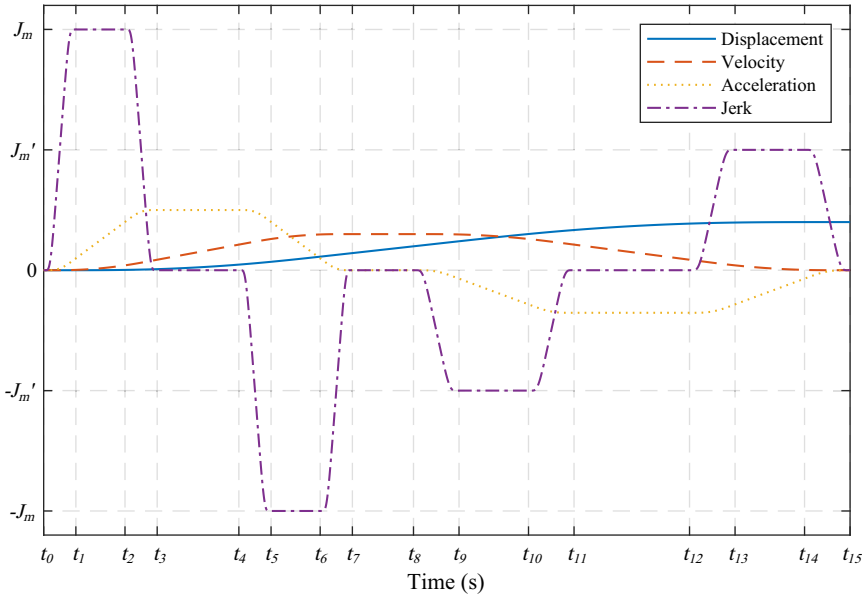
Figure 2. *Kinematic profiles for the normal case of the proposed asymmetric S-curve models.*

As shown in Fig. 2, the idea of the asymmetric profile is to decrease as much as possible the maximum allowable jerk in the deceleration stage without affecting the acceleration stage. Thus, the maximum allowable jerk in the acceleration stage is determined by the maximum capability of the actuator, while the maximum allowable jerk in the deceleration stage can be defined manually, or with the purpose of satisfying the minimum execution time. $I_1 = I_3 = I_5 = I_7$ and $I_2 = I_6$ are set for the acceleration stage $[t_0, t_7]$ to have the null acceleration at the time instant of t_7. Correspondingly, the deceleration stage $[t_8, t_{15}]$ has $I_9 = I_{11} = I_{13} = I_{15}$ and $I_{10} = I_{14}$. The shape of trajectory depends on the actual maximum jerks in the acceleration and deceleration stages. Moreover, it also depends on seven time intervals, which are composed of the varying jerk intervals I_s and I'_s, the constant jerk intervals I_j and I'_j, the constant acceleration intervals I_a and I'_a, and the constant velocity interval I_v. Then, the total execution time I_{total} is the sum of the time intervals of all the fifteen phases:

$$I_{total} = \sum_{i=1}^{15} I_i = 4(I_s + I'_s) + 2(I_j + I'_j) + I_a + I'_a + I_v.$$

The objective of the asymmetric S-curve trajectory planning is to calculate the time intervals I_s, I'_s, I_j, I'_j, I_a, I'_a and I_v to optimize the total execution time under the given kinematic constraints. Acceleration $a(t)$, velocity $v(t)$ and displacement functions $d(t)$ cannot be given analytically, for it is impossible to integrate this jerk function. However, the values of these kinematic variables at every connection time instant can be numerically calculated as the area values under the curve of their derivatives. When the trajectory consists of fifteen segments as shown in Fig. 2, the following relationships between the kinematic values and time intervals hold:

$$\begin{cases} A_m = a(t_3) = a(t_4) = J_m(I_s + I_j) \\ A'_m = a(t_{11}) = a(t_{12}) = J'_m(I'_s + I'_j) \\ V_m = v(t_7) = v(t_8) = A_m(2I_s + I_j + I_a) = A'_m(2I'_s + I'_j + I'_a) \\ |D| = |d(15)| = V_m[2(I_s + I'_s) + I_j + I'_j + \frac{1}{2}(I_a + I'_a) + I_v] \end{cases} \tag{3}$$

where V_m, A_m and J_m are the maximum allowable values within the capability of the actuator, A'_m and J'_m are the maximum allowable acceleration and jerk in the deceleration stage, and D is the travelling distance, representing the displacement relative to the initial and the final position that can be either positive or negative.

The maximum allowable jerk in the deceleration stage is given as follows:

$$J'_m = \lambda J_m \tag{4}$$

Considering the smoothness of deceleration stage, λ is set to be less than 1. In order to achieve the complete closed-form solutions for this asymmetric trajectory, let us assume the relationships between the corresponding time intervals of the acceleration and deceleration stages as follows:

$$\frac{I_s}{I'_s} = \frac{I_j}{I'_j} = \frac{I_a}{I'_a} = k \tag{5}$$

By substituting Eq. (4) and Eq. (5) into Eq. (3), the following equation is derived:

$$
\begin{aligned}
&A_m (2I_s + I_j + I_a) = A'_m (2I'_s + I'_j + I'_a) \\
&\Rightarrow J_m (I_s + I_j) (2I_s + I_j + I_a) = J'_m (I'_s + I'_j) (2I'_s + I'_j + I'_a) \\
&\Rightarrow J_m (I_s + I_j) (2I_s + I_j + I_a) = \frac{1}{k^2} \lambda J_m (I_s + I_j) (2I_s + I_j + I_a) \\
&\Rightarrow k^2 = \lambda \\
&\Rightarrow k = \sqrt{\lambda}
\end{aligned}
\tag{6}
$$

If the above result is substituted into Eq. (5), then

$$
\begin{cases}
I'_s = \frac{I_s}{\sqrt{\lambda}} \\
I'_j = \frac{I_j}{\sqrt{\lambda}} \\
I'_a = \frac{I_a}{\sqrt{\lambda}}
\end{cases}
\tag{7}
$$

Fang et al. [8] decided $\xi = \sqrt{3}/2$ in Eq. (1) under the assumption that the maximum snap should be as small as possible when the execution time and jerk constraints are constant. In the proposed method, $\xi = \sqrt{3}/2$ is used. Then, in the case that the maximum snap in the acceleration stage is constrained by the given S_m, the relationship between S_m and the actual maximum jerk is defined as:

$$j_m = \frac{S_m I_s}{\sqrt{3}} \tag{8}$$

Similarly, it is also defined as $j'_m = S'_m I'_s / \sqrt{3}$ in the deceleration stage.

Because the snap has the direct interrelation with the jerk varying period, then the trade-off between the time optimality and the smoothness can be controlled by S_m.

$$
\begin{aligned}
&\lambda = \frac{j'_m}{j_m} = \frac{\frac{S'_m I'_s}{\sqrt{3}}}{\frac{S_m I_s}{\sqrt{3}}} = \frac{S'_m I'_s}{S_m I_s} = \frac{S'_m}{k S_m} = \frac{S'_m}{\sqrt{\lambda} S_m} \\
&\Rightarrow S'_m = \lambda^{\frac{3}{2}} S_m
\end{aligned}
\tag{9}
$$

The other actual maximum kinematic values can be written as:

$$
\begin{cases}
a_m = \frac{S_m I_s}{\sqrt{3}} (I_s + I_j) \\
a'_m = \frac{S'_m I'_s}{\sqrt{3}} (I'_s + I'_j) \\
v_m = \frac{S_m I_s}{\sqrt{3}} (I_s + I_j) (2I_s + I_j + I_a) = \frac{S'_m I'_s}{\sqrt{3}} (I'_s + I'_j) (2I'_s + I'_j + I'_a) \\
d_m = \frac{S_m I_s}{\sqrt{3}} (I_s + I_j) (2I_s + I_j + I_a) \left[2(I_s + I'_s) + I_j + I'_j + \frac{1}{2} (I_a + I'_a) + I_v \right]
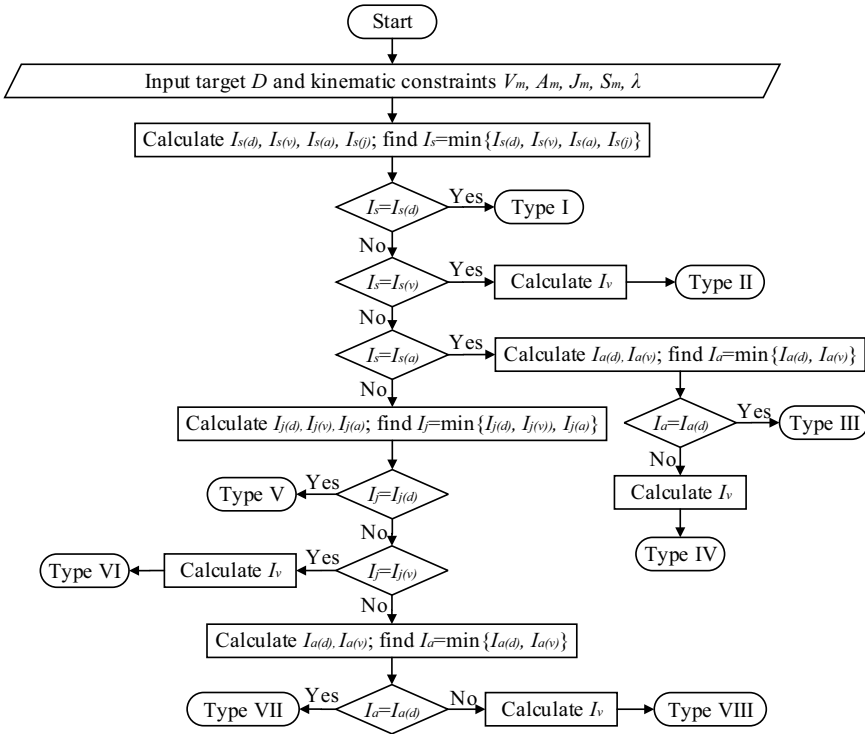\end{cases}
\tag{10}
$$

Figure 3. *Calculation flowchart of algorithm.*

Substituting Eq. (7) into Eq. (10), Eq. (11) is obtained.

$$
\begin{cases}
a_m = \frac{S_m I_s}{\sqrt{3}} \left(I_s + I_j \right) \\
a'_m = \sqrt{\frac{\lambda}{3}} S_m I_s \left(I_s + I_j \right) \\
v_m = \frac{S_m I_s}{\sqrt{3}} \left(I_s + I_j \right) \left(2I_s + I_j + I_a \right) \\
d_m = \frac{S_m I_s}{\sqrt{3}} \left(I_s + I_j \right) \left(2I_s + I_j + I_a \right) \left[\left(1 + \frac{1}{\sqrt{\lambda}} \right) \left(2I_s + I_j + \frac{1}{2} I_a \right) + I_v \right]
\end{cases}
\tag{11}
$$

Once the time intervals in the acceleration stage are determined, the corresponding values of the deceleration stage are obtained by them from Eq. (8), Eq. (10) and Eq. (11). Hence, in the following subsection, the time intervals in the acceleration stage are calculated to obtain the optimal execution time of the motion.

2.2. Calculation of time intervals

There exists no systematic method to find a time-optimal value for S-curve trajectory planning under the kinematic constraints. In the practical applications, the time intervals I_j, I_a and I_v may exist or not for achieving the optimal execution time under the target displacement and the kinematic limits. Only the jerk varying interval I_s exists in generating the trajectory. All possible cases can be divided into eight types. In order to obtain the case with optimal execution time out of eight cases, four steps are set below. Figs. 3-4 show the flowchart of algorithm and all the possible jerk profiles.

Step 1: Determination of the varying jerk interval I_s

(I) Firstly, the relationship between the target distance $d(t_{15})$ with the specific limit of snap, S_m and the time interval I_s is established from Eq. (13) under the assumption without exceeding the constraints of jerk, acceleration and velocity.
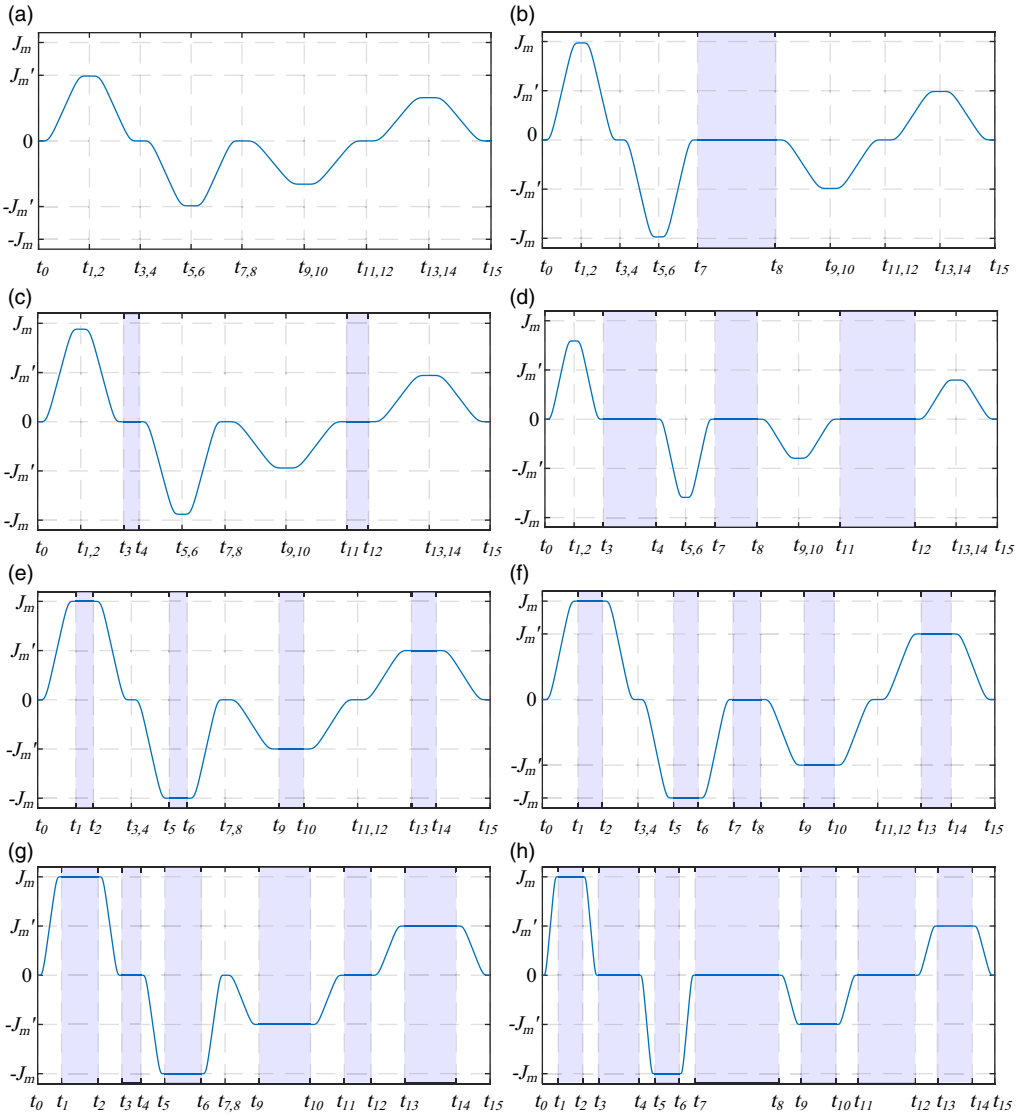
Figure 4. *Jerk profile models: (a) Type I; (b) Type II; (c) Type III; (d) Type IV; (e) Type V; (f) Type VI; (g) Type VII; (h) Type VIII.*

This includes that I_j, I_a and I_v don't exist.

$$d_m = \left| d(t_{15} | I_j = I_a = I_v = 0) \right| = \frac{4 \left(1 + \frac{1}{\sqrt{\lambda}} \right) S_m I_s^4}{\sqrt{3}} \tag{12}$$

To obtain the target distance, the left side is set to be D and the additional subscript is added to distinguish the values of I_s calculated with the different constraints below. Then I_s decided by the displacement is as follows:

$$I_{s(d)} = \sqrt[4]{\frac{\sqrt{3} \, |D|}{4 \left(1 + \frac{1}{\sqrt{\lambda}} \right) S_m}} \tag{13}$$

This value can be broken by the given kinematic constraints and so it is essential to confirm the upper bound of I_s related with them.

(II) Then, the maximum velocity limit is introduced. It is clear that the maximum velocity is achieved at the time t_7. That is,

$$v_m = v(t_7 | I_j = I_a = 0) = \frac{2S_m I_s^3}{\sqrt{3}} \tag{14}$$

v_m should not be larger than the velocity constraint V_m of the actuator and the limit of corresponding period I_s is obtained as

$$I_{s(v)} = \sqrt[3]{\frac{\sqrt{3}V_m}{2S_m}} \tag{15}$$

(III) Next, the constraint of maximum acceleration should be considered. The acceleration reaches the maximum at the time I_s.

$$a_m = a(t_3 | I_j = 0) = \frac{S_m I_s^2}{\sqrt{3}} \tag{16}$$

Considering the acceleration constraint, a_m sets to be A_m. Thus, I_s is calculated as follows:

$$I_{s(a)} = \sqrt{\frac{\sqrt{3}A_m}{S_m}} \tag{17}$$

(IV) Finally, I_s constrained by jerk bound can be derived directly from Eq. (8).

$$I_{s(j)} = \frac{\sqrt{3}J_m}{S_m} \tag{18}$$

I_s from Eq. (19) satisfies all constraints and is used in the rest steps.

$$I_s = \min\{I_{s(d)}, I_{s(v)}, I_{s(a)}, I_{s(j)}\} \tag{19}$$

Then there exist four possible values for I_s.

Case 1: If $I_{s(d)} = \min\{I_{s(d)}, I_{s(v)}, I_{s(a)}, I_{s(j)}\}$, the time interval existing during the motion is only the varying jerk interval and $I_j = I_a = I_v = 0$. Then, the actual maximum velocity, acceleration, jerk and the total execution time are as Eq. (20) and complete to calculate.

$$j_m = \frac{S_m I_{s(d)}}{\sqrt{3}} \tag{20}$$

Case 2: If $I_{s(v)} = \min\{I_{s(d)}, I_{s(v)}, I_{s(a)}, I_{s(j)}\}$, the actual maximum velocity is reached while the maximum acceleration and jerk aren't reached. Thus $I_j = I_a = 0$ and the actual maximum jerk is calculated by Eq. (21). Go to step 4.

$$j_m = \frac{S_m I_{s(v)}}{\sqrt{3}} \tag{21}$$

Case 3: If $I_{s(a)} = \min\{I_{s(d)}, I_{s(v)}, I_{s(a)}, I_{s(j)}\}$, $I_j = 0$. The constant jerk interval disappears by the acceleration constraint. Then, the actual maximum jerk is calculated by Eq. (22). Go to step 3.

$$j_m = \frac{S_m I_{s(a)}}{\sqrt{3}} \tag{22}$$

Case 4: If $I_{s(j)} = \min\{I_{s(d)}, I_{s(v)}, I_{s(a)}, I_{s(j)}\}$, the actual maximum jerk is equal to the maximum allowable jerk, that is $j_m = J_m$. Then go to step 2.

Step 2: Determination of the constant jerk interval I_j

(I) Supposing that the acceleration and velocity constraints are satisfied, we start to calculate I_j with the relationship between the final displacement and I_j.

$$|d(t_{15}|I_a = I_v = 0)| = |D| = j_m\left(4I_s^3 + 8I_s^2 I_j + 5I_s I_j^2 + I_j^3\right)\left(1 + \tfrac{1}{\sqrt{\lambda}}\right)$$

$$\Rightarrow I_{j(d)} = \sqrt[3]{\frac{I_s^3}{27} + \frac{|D|}{2\left(1+\frac{1}{\sqrt{\lambda}}\right)j_m} + \sqrt{\frac{|D|}{27\left(1+\frac{1}{\sqrt{\lambda}}\right)j_m} + \frac{D^2}{4\left(1+\frac{1}{\sqrt{\lambda}}\right)^2 j_m^2}}}$$

$$+ \sqrt[3]{\frac{I_s^3}{27} + \frac{|D|}{2\left(1+\frac{1}{\sqrt{\lambda}}\right)j_m} - \sqrt{\frac{|D|}{27\left(1+\frac{1}{\sqrt{\lambda}}\right)j_m} + \frac{D^2}{4\left(1+\frac{1}{\sqrt{\lambda}}\right)^2 j_m^2}}} - \frac{5I_s}{3} \tag{23}$$

Since I_s and j_m were decided in Step 1, from now on, we use j_m instead of $S_m I_s / \sqrt{3}$ in Eq. (11).

(II) I_j under the velocity constraint is obtained as:

$$v(t_7|I_a = 0) = V_m = j_m\left(2I_s^2 + 3I_s I_j + I_j^2\right)$$

$$\Rightarrow I_{j(v)} = -\frac{3I_s}{2} + \sqrt{\frac{I_s^2}{4} + \frac{V_m}{j_m}} \tag{24}$$

(III) I_j under the acceleration constraint is calculated as follows:

$$a(t_3) = A_m = j_m\left(I_j + I_s\right)$$

$$\Rightarrow I_{j(a)} = -\frac{A_m}{j_m} - I_s \tag{25}$$

Then, the constant jerk interval I_j is selected by Eq. (26) and

$$I_j = \min\left\{I_{j(d)},\ I_{j(v)},\ I_{j(a)}\right\} \tag{26}$$

Then, there exists three possible values for I_j.

Case 1: If $I_{j(d)} = \min\{I_{j(d)}, I_{j(v)}, I_{j(a)}\}$, $I_a = I_v = 0$. Then, the actual maximum velocity, acceleration and the total execution time are as Eq. (27) and complete to calculate.

$$\begin{cases} a_m = j_m\left(I_s + I_{j(d)}\right) \\ v_m = j_m\left(I_s + I_{j(d)}\right)\left(2I_s + I_{j(d)}\right) \\ I_{total} = \left(4I_s + 2I_{j(d)}\right)\left(1 + 1/\sqrt{\lambda}\right) \end{cases} \tag{27}$$

Case 2: If $I_{j(v)} = \min\{I_{j(d)}, I_{j(v)}, I_{j(a)}\}$, then $I_a = 0$. Therefore, the acceleration does not need to reach its maximum for achieving the maximum allowable velocity. Then, the actual maximum velocity and acceleration are given as Eq. (28) and go to Step 4.

$$\begin{cases} a_m = j_m\left(I_s + I_{j(v)}\right) \\ v_m = j_m\left(I_s + I_{j(v)}\right)\left(2I_s + I_{j(v)}\right) \end{cases} \tag{28}$$

Case 3: If $I_{j(a)} = \min\{I_{j(d)}, I_{j(v)}, I_{j(a)}\}$, $a_m = A_m$. Go to Step 3.

Step 3: Determination of the constant acceleration interval I_a

(I) Supposing that the velocity constraint satisfies, the interval I_a is calculated by the following Eq. (29).

$$|d(t_{15}|I_v = 0)| = |D| = \frac{1+\frac{1}{\sqrt{\lambda}}}{2} a_m\left(I_a^2 + 3I_j I_a + 6I_s I_a + 8I_s^2 + 2I_j^2 + 8I_s I_j\right)$$

$$\Rightarrow I_{a(d)} = \frac{-\left(6I_s + 3I_j\right) + \sqrt{\left(2I_s + I_j\right)^2 + \frac{8|D|}{\left(1+\frac{1}{\sqrt{\lambda}}\right)a_m}}}{2} \tag{29}$$

(II) Then, we calculate I_a by the velocity constraint.

$$v(t_7) = V_m = a_m\left(I_a + 2I_s + I_j\right)$$

$$\Rightarrow I_{a(v)} = \frac{V_m}{a_m} - 2I_s - I_j \tag{30}$$

Then, we decide the minimum I_a from the Eq. (31).

$$I_a = \min\{I_{a(d)},\ I_{a(v)}\} \tag{31}$$

Then, there exists two possible values for I_a.

Case 1: If $I_{a(d)} = \min\{I_{a(d)},\ I_{a(v)}\}$, $I_v = 0$ and the trajectory type is decided. The interval in which the velocity is the maximum allowable value is disappeared. The actual velocity v_m and the total execution time are calculated as:

$$\begin{cases} v_m = a_m\left(2I_s + I_j + I_{a(d)}\right) \\ I_{total} = \left(4I_s + 2I_j + I_{a(d)}\right)\left(1 + \sqrt{\lambda}\right) \end{cases} \tag{32}$$

Case 2: If $I_{a(v)} = \min\{I_{a(d)},\ I_{a(v)}\}$, $v_m = V_m$. Go to the step 4.

Step 4: Determination of the constant velocity interval I_v

The constant velocity interval, I_v is calculated in Eq. (33) on the basis of the target distance and the already calculated time intervals.

$$I_v = \frac{|D - d(t_{15}|I_v = 0)|}{v_m} = \frac{|D|}{v_m} - \left(1 + \frac{1}{\sqrt{\lambda}}\right)\left(2I_s + I_j + \frac{I_a}{2}\right) \tag{33}$$

According to Steps 1-4, the time intervals I_s, I_j, I_a and I_v have the complete closed-form solutions to decide the S-curve trajectory. This algorithm not only covers all the possible profile types but also calculates the optimal execution time subject to the different kinematic constraints.

2.3. Estimation of an asymmetric parameter λ

The execution time varies under the identical kinematic constraints according to the values of the asymmetric parameter λ and the specific snap (the maximum snap of the acceleration or deceleration stage). According to Eq. (7), Eq. (9) and $0 < \lambda \le 1$, the maximum snap of the deceleration stage is not always larger than one of the acceleration stage and the execution time of the deceleration stage is always more lengthened than one of the acceleration stage. Fig. 5 illustrates the variation of the execution time according to λ when the maximum snap of the acceleration and deceleration stage is specified respectively. Here, T is the total execution time of the symmetric profile ($\lambda = 1$).

If the maximum snap of the acceleration stage sets up to be a specified value, the motion time of the acceleration stage is always fixed and the motion time of the deceleration stage is lengthened than the one of the acceleration stage according to $0 < \lambda \le 1$. Then, the total execution time is increased as λ is decreased, while it is decreased as λ is increased. Thus, the total execution time is more lengthened than one of the symmetric profile ($\lambda = 1$) by Eq. (20), Eq. (27), Eq. (32) and Eq. (33) while the maximum snap of the acceleration stage is the same and the maximum stage of the deceleration stage is shorter. Therefore, the smoother profile is always generated in the asymmetric trajectory. The blue line in Fig. 5 shows the result of the execution time according to λ in the case of specifying the maximum snap of the acceleration stage.

If the maximum snap of the deceleration stage sets up as a specified value, the maximum snap of the acceleration stage is larger than one of the deceleration stage. Then, the cases that the total execution time is smaller than one with $\lambda = 1$ may exist according to λ. Since the maximum snap of the acceleration stage is increased as λ is decreased, the execution time of the acceleration stage is much smaller and therefore the total execution time could be smaller than the symmetric profile according to the execution time of the acceleration stage and λ by Eq. (7) and Eq. (9).

Let us see the relationship between λ and the execution time according to the displacement and snap when giving the kinematic constraints. For example, under the kinematic constraints ($V_m = 10$ rad/s, $A_m = 12$ rad/s^2, $J_m = 40$ rad/s^3 and $S_{dm} = 150$ rad/s^4), the variation curve between λ and the execution time according to the displacement is shown in Fig. 6 below.
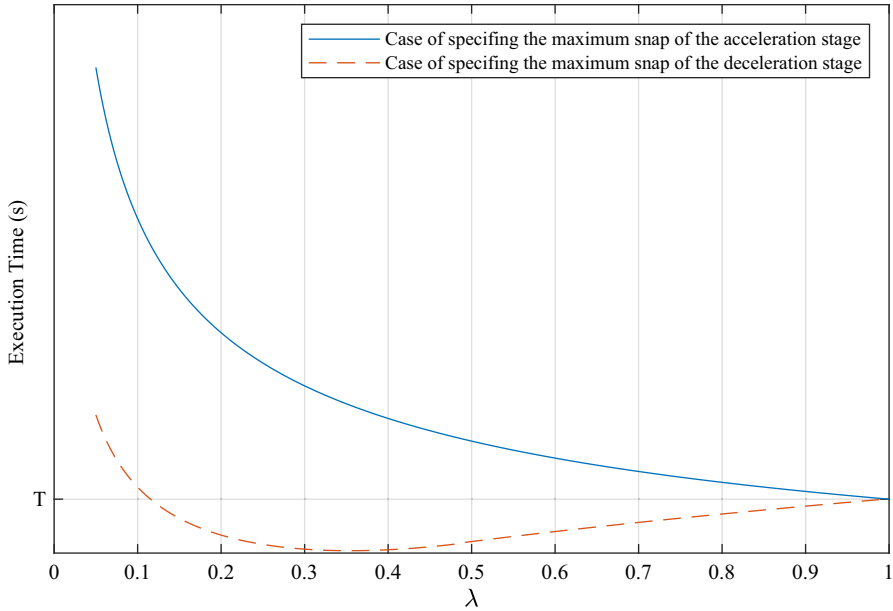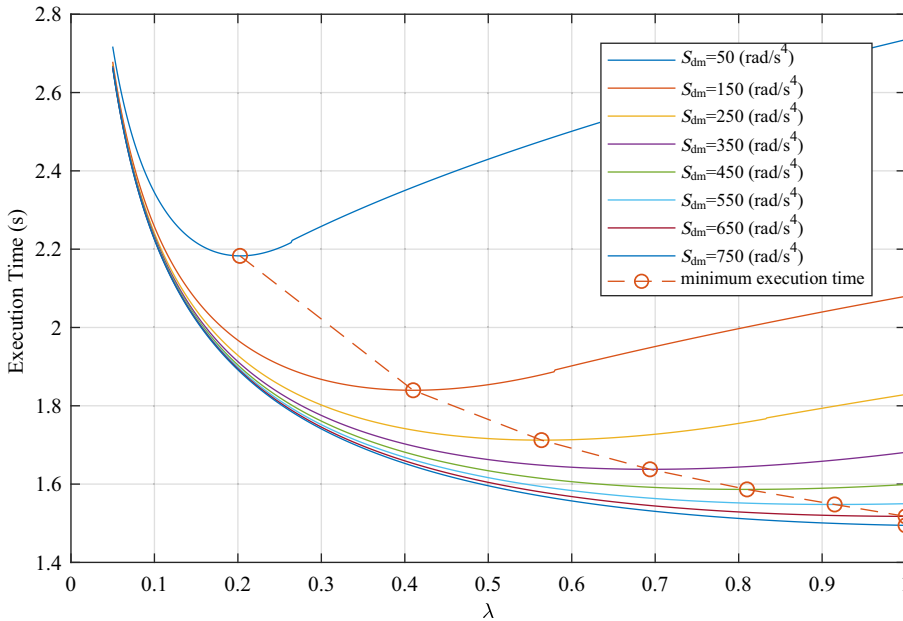
Figure 5. *Variation curve of execution time according to λ when the maximum snap of the acceleration and deceleration stage is specified.*
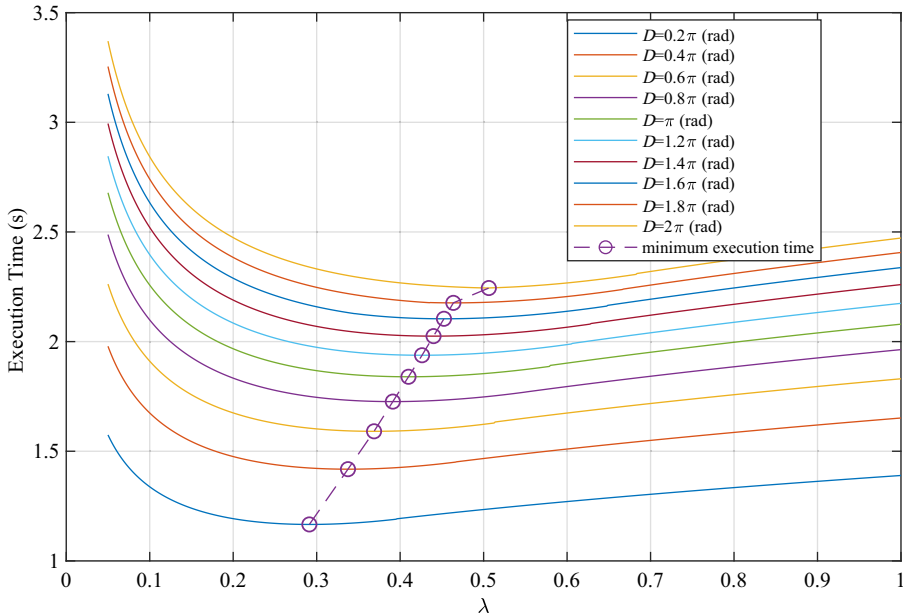
Figure 6. *Variation curve between the asymmetric parameter λ and the execution time according to the displacement ($V_m = 10$ rad/s, $A_m = 12$ rad/s², $J_m = 40$ rad/s³, $S_{dm} = 150$ rad/s⁴).*

As shown in Fig. 6, when the displacement isn't so large, λ of achieving the minimum execution time is close to zero and increases gradually as the displacement is lengthened. But even though the displacement is very large, it might be impossible to achieve the minimum execution time for $λ = 1$ due to the relationship between the kinematic constraints (velocity, acceleration and jerk). Fig. 7 shows the relationship between λ and the execution time according to the maximum snap of the deceleration stage

Figure 7. *Variation curve of the execution time versus the asymmetric parameter λ according to the maximum snap of the deceleration stage ($D = \pi\,rad$, $V_m = 10\,rad/s$, $A_m = 12\,rad/s^2$, $J_m = 40\,rad/s^3$, $S_{dm} = 150\,rad/s^4$).*

when giving the kinematic constraints (displacement, velocity, acceleration and jerk). As illustrated in Fig. 7, λ achieving the minimum execution time is small as the maximum snap of the deceleration stage is decreased and inversely λ is approaching 1 as the snap is increased. If the maximum snap of the deceleration stage is larger than a certain value, the required λ is equal to 1.

Hence, the minimum execution time is generated in the same model as the symmetric profile. But the large threshold of snap is not prerequisite, because the purpose of this article is to enhance the effectiveness of the motion more in the operation of attaching importance to the smoothness of the motion. As the kinematic indices (velocity, acceleration and jerk) reached their limits, the efficiency is more increased but the smoothness of the motion is more decreased, if the bounded value of snap is very large.

It is difficult to calculate the asymmetric parameter λ analytically. This article presents an algorithm to get the asymmetric parameter λ for achieving the minimum execution time under the kinematic constraints when restricting the maximum snap of the deceleration stage.

As shown in Fig. 6, we decide the asymmetric parameter λ according to the previously given displacement using the algorithm and may use the values effectively in the online control.

2.4. Synchronization of multi-axis motions

When λ is given the certain value, the time-scaled synchronization and velocity synchronization method presented in ref. [8] can be applied to this trajectory planning method for synchronization of multi-axis motions. As above-mentioned, when limiting the maximum snap of the deceleration stage, not only the smoother profile is generated than the symmetric profile in the deceleration stage, but the motion time can be more decreased. Algorithm 2 presents the calculation procedure for generating a time-scaled synchronized trajectory using algorithm 1.

Algorithm 1: Decision of λ satisfying the minimum execution time

Input:
(1) asymmetric parameter step value $step_\lambda$
(2) The required displacements D, kinematic constraints V_m, A_m, J_m, and the snap limit in the deceleration stage S_{dm}

Output: The asymmetric parameter λ

1:    $\lambda_{temp} = 1$;
2:    $Calc_tf = $ true;
3:    while $Calc\_tf$ do
4:        $S_{am} = S_{dm}/\lambda_{temp} \wedge (3/2)$;
5:        Compute the time parameters (T_s, T_j, T_a, T_v) and execution time T_{exe} with
        $(D, V_m, A_m, J_m, S_{am}, \lambda_{temp})$;
6:        if $\lambda_{temp} == 1$ then
7:           $\lambda = 1; T_{\min\_exe} = T_{exe}$;
8:        else
9:           if $T_{exe} \leq T_{\min\_exe}$ then
10:             $\lambda = \lambda_{temp}; T_{\min\_exe} = T_{exe}$;
11:           else
12:             $Calc_tf = $ false;
13:           end if
14:        end if
15:        $\lambda_{temp} = \lambda_{temp} - step_\lambda$;
16: end while
17: return λ

Algorithm 2: Calculation procedure for time-scaled synchronized trajectory generation

1:    Calculate the minimum execution time $T_{\min\_exe,k}$ and time parameters $(T_{s,k}, T_{j,k}, T_{a,k}, T_{v,k})$ using algorithm 1 for all joints under the kinematic constraints
     $(D_k, V_{m,k}, A_{m,k}, J_{m,k}, S_{dm,k})(k = 1, 2, \cdots, N)$.
2:    $T_{\min\_exe}^{sync} = \max \{T_{\min\_exe,1}, T_{\min\_exe,2}, \cdots, T_{\min\_exe,N}\}$
3:    for $k = 1$ to N do
4:        $\gamma_k = T_{\min\_exe}^{sync}/T_{\min\_exe,k}$;
5:        $(T_{s,k}^{sync}, T_{j,k}^{sync}, T_{a,k}^{sync}, T_{v,k}^{sync}) = \gamma_k(T_{s,k}, T_{j,k}, T_{a,k}, T_{v,k})$;
6:        $j_{m,k}^{sync} = j_{m,k}/\gamma_k^3$;
7:    end for
8:    return $\{j_{m,k}^{sync}, (T_{s,k}^{sync}, T_{j,k}^{sync}, T_{a,k}^{sync}, T_{v,k}^{sync})\}(k = 1, 2, \cdots, N)$

---

3. Results and discussion

3.1. 3 DOF robotic manipulator: trajectory planning on a straight line motion of the end-effector in the task space

Firstly, we consider 3 DOF robotic manipulator as the typical case, where we generate a straight line motion of the end-effector in the task space. The coordinates and displacements of the initial and end points of the end-effector are given in Table I.

The diagram of this robotic manipulator and rectilinear motion trajectory in the Cartesian coordinate are shown in Fig. 8.

Xiao et al. and Fang et al. already performed the trajectory planning with the task data [8, 10]. Based on this, we generate the trajectories with the constraints shown in Table II to illustrate the asymmetric S-curve trajectories under the different kinematic constraints. Then, for asymmetry, the jerks given in

Table I. *End-effector coordinates at the initial and end points and corresponding displacements.*

Axis	Initial point (m)	End point (m)	Displacement (m)
x	0.15	0	−0.15
y	0	1.3	1.3
z	0.4	0.9	0.5
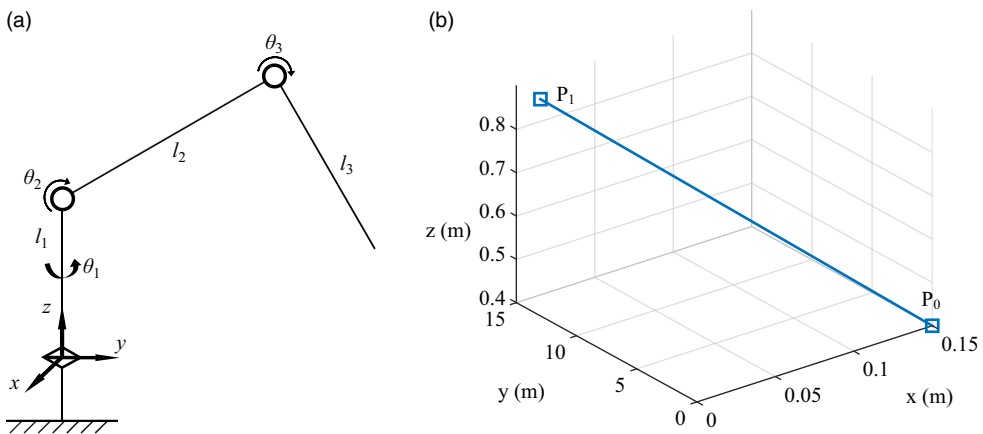
Figure 8. *(a) Diagram of 3 DOF robotic manipulator; (b) rectilinear motion trajectory in the Cartesian coordinate (P_0-initial point, P_1-end point).*

Table II are set to be the maximum allowable jerks in the acceleration stage and the maximum allowable jerks in the deceleration stage equal to the halves of jerks in the acceleration stage. The maximum allowable snap of the acceleration stage is set to be $275.22 m/s^4$, $125.10 m/s^4$ and $41.70 m/s^4$ in the three constraint sets, respectively. Then, the allowable maximum snaps of the deceleration stage are obtained from Eq. (4) and Eq. (9) directly.

Figs. 9-13 illustrate the trajectories of displacements, velocities, accelerations, jerks and snaps of the end-effector about every axis and angle position trajectories of every joint are shown in Fig. 14.

Since the displacement, velocity, acceleration and jerk trajectories of end-effector are continuous and zero at the initial moment and final moment of motion as illustrated in Figs. 9-14, the end-effector moves smoothly under the given constraints.

Therefore, impulses can be avoided and it is favourable to the exact control of the joints.

3.2. 6 DOF robotic manipulator: the synchronized trajectory planning in the joint space

We apply the proposed method to the trajectory planning of the 6 DOF robotic manipulator. Then, the trajectory is generated in the joint space. The simulation data is set to be identical to the data in refs. [8, 30, 39]. Table III shows the kinematic constraints and positions of joints.

The maximum allowable jerk in the acceleration stage is equal to the data given in Table III. Also, the snap constraints in the deceleration stage are set to be 150 rad/s⁴. Then, the snap constraints in the acceleration stage are determined by Eq. (9) and λ obtained using the algorithm 1. Table IV shows the comparative results of the execution time with the real maximum jerk of joints in the unsynchronized case in ref. [8]. As can be shown in Table IV, the execution times of all joints are smaller and the real maximum jerks are shortened about 30% lower than that of the trajectories presented in ref. [8].

***Table II.*** *Kinematic constraints of the robot along every axis in the task space.*

Kinematic constraints	Velocity (m/s)			Acceleration (m/s2)			Jerk (m/s3)		
	Axis *x*	Axis *y*	Axis *z*	Axis *x*	Axis *y*	Axis *z*	Axis *x*	Axis *y*	Axis *z*
Set 1	0.10	0.83	0.32	0.23	2.00	0.77	1.29	11.26	4.33
Set 2	0.11	0.94	0.36	0.21	1.83	0.71	0.86	7.49	2.88
Set 3	0.14	1.26	0.48	0.22	1.91	0.73	0.68	5.90	2.27
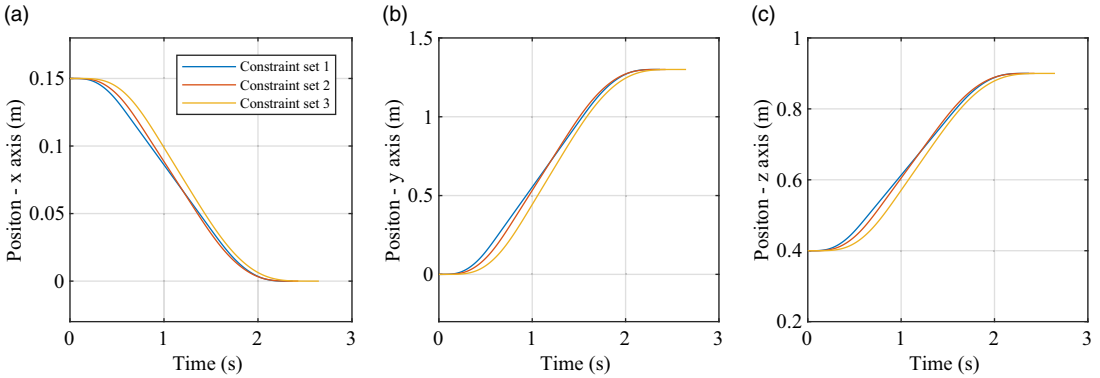
Figure 9. *End-effector displacement trajectories about (a) x-axis; (b) y-axis; and (c) z-axis.*
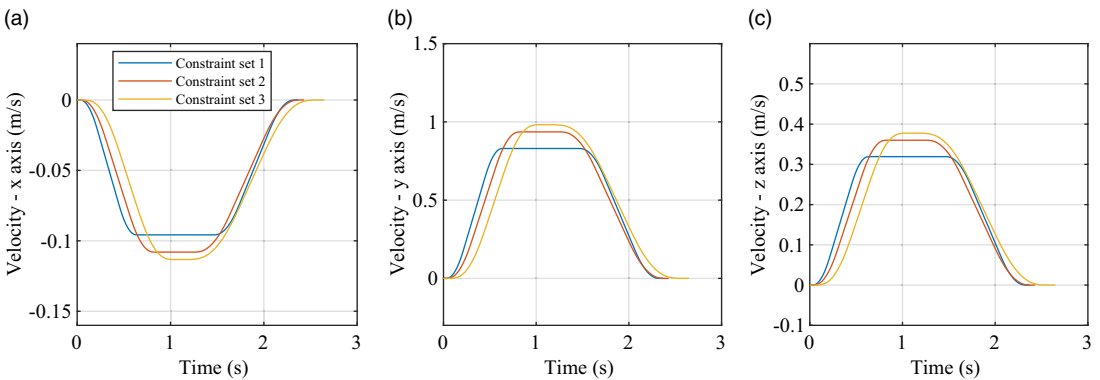
Figure 10. *End-effector velocity trajectories about (a) x-axis; (b) y-axis; and (c) z-axis.*
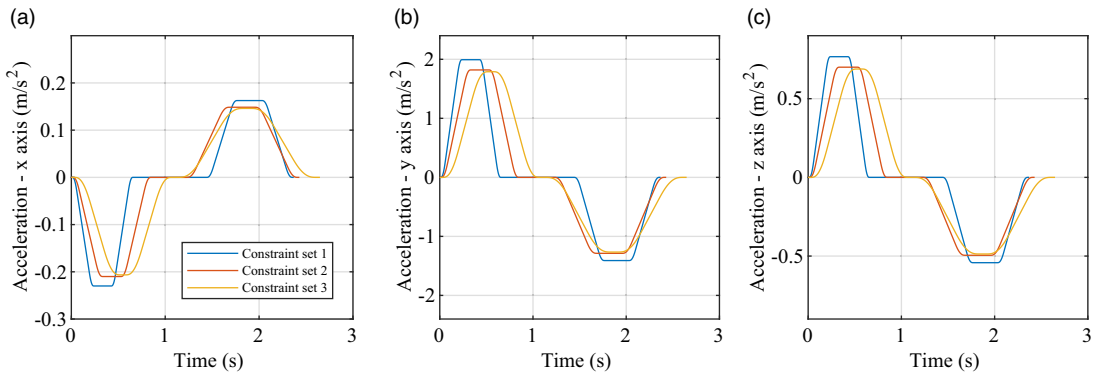
Figure 11. *End-effector acceleration trajectories about (a) x-axis; (b) y-axis; and (c) z-axis.*
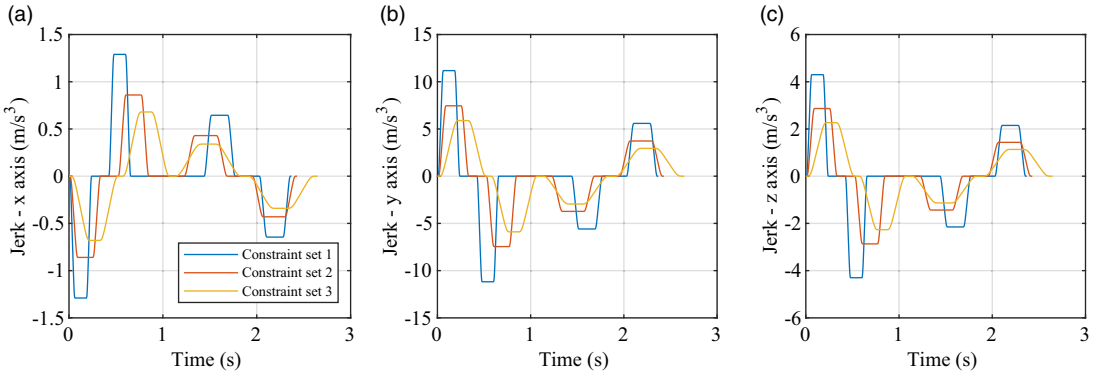
Figure 12. *End-effector jerk trajectories about (a) x-axis; (b) y-axis; and (c) z-axis.*
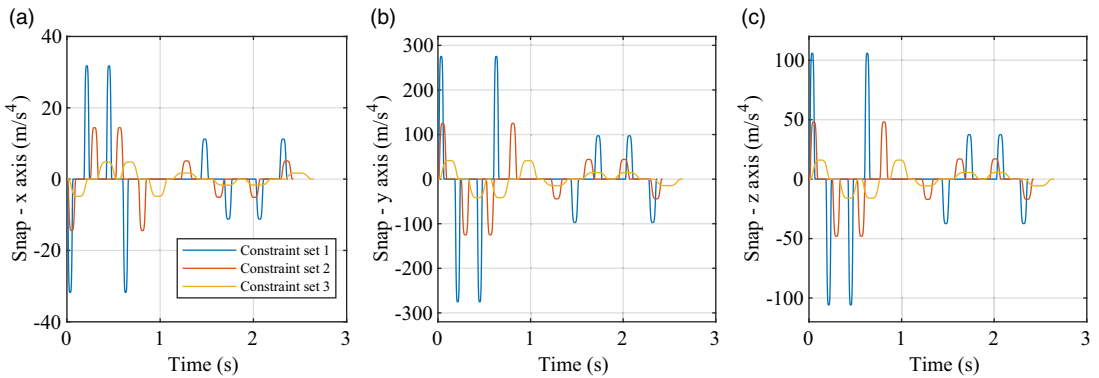
Figure 13. *End-effector snap trajectories about (a) x-axis; (b) y-axis; and (c) z-axis.*
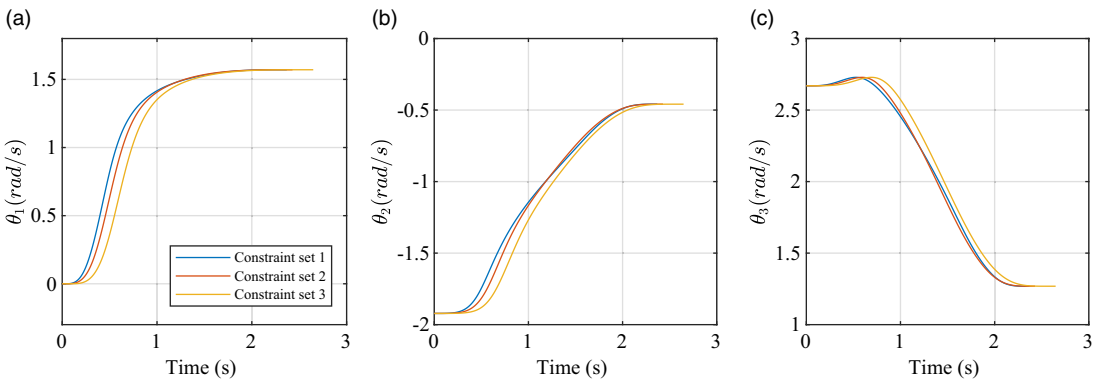

Figure 14. *Angle position trajectories of (a) joint 1; (b) joint 2; and (c) joint 3.*

Table V illustrates the comparative results of the real maximum jerk and snap of joints in the time-scaled synchronized case with respect to that in ref. [8]. As shown in Table V, it can be seen that the real maximum jerk and snap of all joints in the deceleration stage are much smaller.

Fig. 15 shows the results given by the time-scaled synchronization method proposed in this paper.

The position, velocity, acceleration and jerk of all the joints satisfy the kinematical constraints in Table III, and the trajectories are smooth and continuous during the whole motion. And Fig. 16 shows

Table III. *Positions and kinematic constraints of the robot joints.*

		Joint					
		1	**2**	**3**	**4**	**5**	**6**
Positions (rad)	Initial point (rad)	0	$-\pi/6$	0	$-\pi/3$	0	0
	Final point (rad)	$2\pi/3$	$\pi/6$	$\pi/4$	$\pi/3$	$-\pi/4$	$\pi/6$
Kinematic constraints	Velocity (rad/s)	8	10	10	5	5	5
	Acceleration (rad/s^2)	10	12	12	8	8	8
	Jerk (rad/s^3)	30	40	40	20	20	20

Table IV. *Comparative results of the execution time and the jerk of joints in the unsynchronized case.*

	Calculation by [8]		Calculation by Algorithm 1	
Joint	Execution time(s)	Actual maximum jerk (rad/s³)	Execution time (s)	Actual maximum jerk in the deceleration stage (rad/s³)
1	1.8759 (100%)	20.3067 (100%)	1.7071 (91%)	14.3659 (70.7%)
2	1.5774 (100%)	17.0759 (100%)	1.3470 (85.4%)	12.9960 (76.1%)
3	1.4679 (100%)	15.8909 (100%)	1.2419 (84.6%)	12.2324 (77.0%)
4	1.8760 (100%)	20.0000 (100%)	1.8163 (96.8%)	13.4152 (67.0%)
5	1.4679 (100%)	15.8909 (100%)	1.3681 (93.2%)	10.9520 (68.9%)
6	1.3264 (100%)	14.3590 (100%)	1.2176 (91%)	10.0536 (70.0%)

Table V. *Comparative results of the jerk and snap of joints calculated by the time-scaled synchronization.*

	Calculation by [8]		Calculation by Algorithm 2	
Joint	Jerk (rad/s³)	Snap (rad/s⁴)	Maximum Jerk in the deceleration stage(rad/s³)	Maximum Snap in the deceleration stage(rad/s⁴)
1	20.3032 (100%)	149.9655 (100%)	11.9282 (58.7%)	117.0615 (78.0%)
2	10.1516 (100%)	74.9828 (100%)	5.3009 (52.2%)	45.3739 (60.5%)
3	7.6137 (100%)	56.2371 (100%)	3.9106 (51.3%)	32.79 (58.3%)
4	20.0000 (100%)	150.000 (100%)	13.4152 (67.0%)	150 (100%)
5	7.6137 (100%)	56.2371 (100%)	4.6806 (61.5%)	48.2878 (85.86%)
6	5.0758 (100%)	37.4914 (100%)	3.0290 (59.6%)	30.2962 (80.8%)

the end-effector trajectories of the UR5 robot manipulator (position, velocity, acceleration and jerk trajectories) in the task space when every joint is moved along the trajectories shown in Fig. 15.

As shown in Fig. 16, since the displacement, velocity, acceleration and jerk trajectories of end-effector are continuous and zero at the initial and final point of motion, the end-effector moves smoothly. Thus, it can be seen that the smooth starting and ending of trajectory could also be ensured.

Also, we analyse the execution time with four different types of trajectories [8, 18, 30, 37] using the kinematical constraints in Table III. We perform the calculation of two cases for the proposed method, where the jerk given in Table III is set to be the allowable maximum jerks of the acceleration stage. For 1ˢᵗ calculation, the maximum snap of the deceleration stage is set to be $150 rad/s^4$ and λ is determined by using the algorithm 1 for every joint. For 2ⁿᵈ calculation, the maximum snap of the acceleration stage is set to be $700 rad/s^4$ and λ is set to be 0.9 for all joints. Then, the maximum snaps of the deceleration or acceleration stage are obtained from Eq. (4) and Eq. (9). Fig. 17 shows the motion profiles of joint 4, which is generated by the benchmark methods and the proposed one. The motion profiles generated
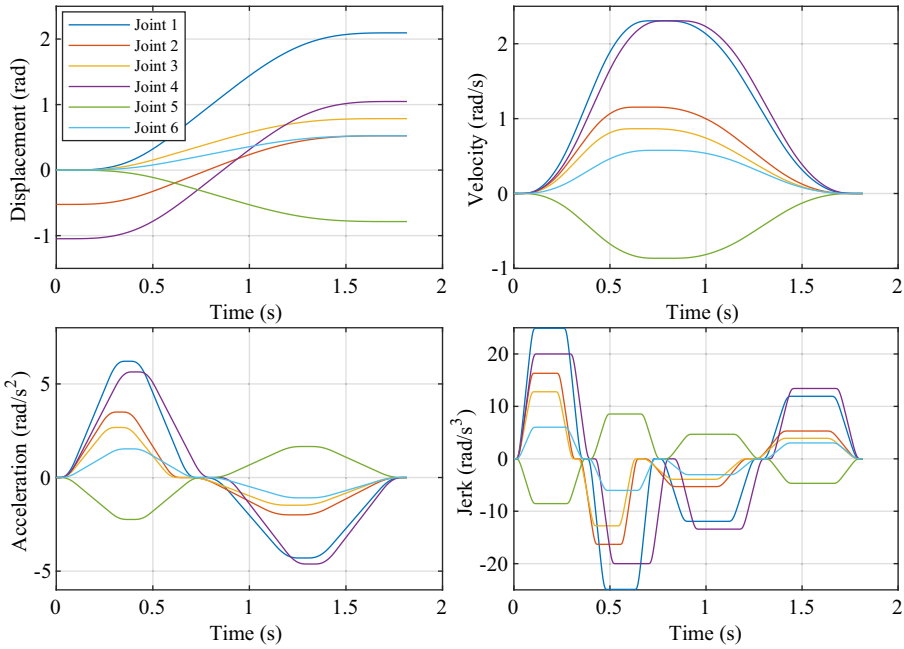
Figure 15. *Asymmetric S-curve profiles generated by new time-scaled synchronization.*
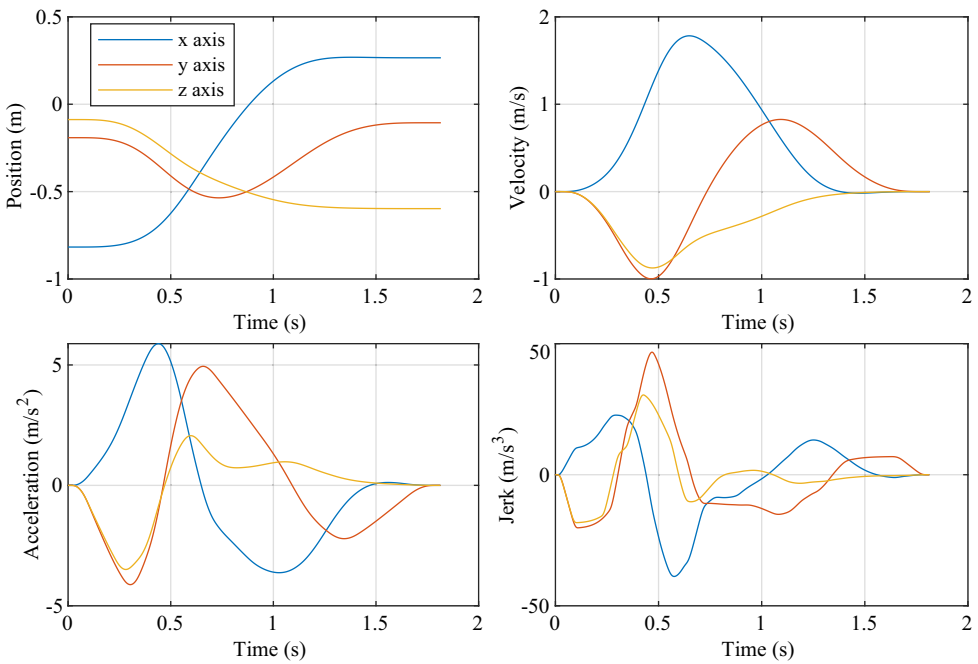

Figure 16. *End-effector trajectories of the 6 DOF robot manipulator.*
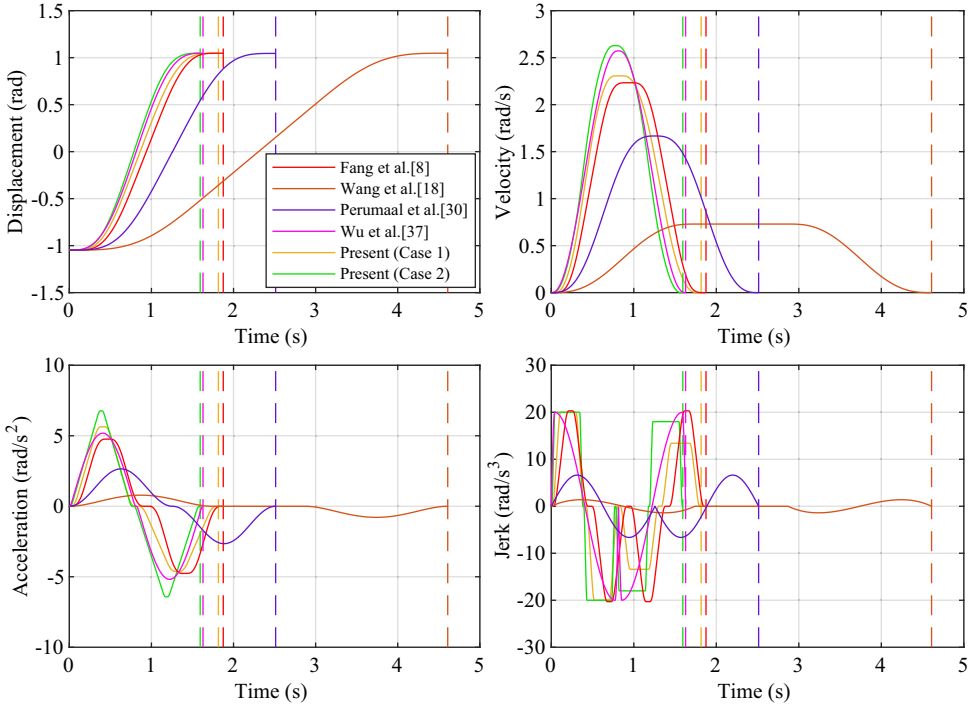
Figure 17. *Motion profiles of joint 4 for different trajectory models.*

by [15] show that the real maximum jerk has the lowest value compared with other algorithms, which resulted in the longest execution time. Table VI presents the measured performances including the execution time and real maximum jerk of acceleration and deceleration stage by the benchmark algorithms and the proposed one for the test task. The results show that the proposed method yielded the smaller execution time than the benchmark ones [8, 18, 30]. Compared with [37], the obtained execution time for 1st calculation is larger, but it is shorter for 2nd calculation. As shown in Table VI and Fig. 17, if the maximum snap is set as a large value relative to the jerk constraints, the jerks will reach the maximal value in a comparatively short period so that the shorter execution time is generated. However, the generated jerk profiles will lead to harmful vibrations. If adjusting the allowable maximum snap and jerk in the deceleration stage, it is possible to control the relationship between the execution time and smoothness.

3.3. Estimation of residual vibration

To assess the efficiency of the proposed method, we have carried out the analysis of residual vibration.

The dynamic model of a simplified single-axis motion stage is shown in Fig. 18. It includes a flexible base structure with a weight of m_1, holding a motor to move a mass with an equivalent weight of m_2. The friction force between the moving mass and the machine base is ignored. The dynamics of the flexible base is assumed to be a single-degree-of-freedom mass-spring-damper system, with a spring stiffness k and damping coefficient c.

Where the moving mass m_2 is driven with an acceleration a, the reaction force on the base structure m_1 will be $F = m_2 a$.

The dynamics of the base structure can be expressed as

$$m_1 \ddot{x} + c\dot{x} + kx = F = m_2 a \tag{34}$$

Table VI. *Comparative results of several planning methods.*

Work	Trajectory model	Execution (s)	Maximum Jerk (rad/s³)	Maximum Jerk in the deceleration stage (rad/s³)
Fang et al. [8]	15-segment sigmoid jerk	1.876	20.30 (Joint 1) ($S_{max} = 150\,rad/s^4$)	20.30 (Joint 1) ($S_{max} = 150\,rad/s^4$)
Wang et al. [18]	High-order polynomial jerk	4.609	1.526 (Joint 1)	1.526 (Joint 1)
Perumaal et al. [30]	3-segment sine jerk (sync acc/dec)	2.513	6.63 (Joint 1, 4)	6.63 (Joint 1, 4)
Wu et al. [37]	Locally asymmetrical 15-segment sine jerk	1.6286 ($\alpha = 1$, $\beta = 0.1$)	20 (Joint 1, 4)	20 (Joint 1, 4)
Present	Asymmetric 15-segment sigmoid jerk	1.816	24.90 (Joint 1) ($S_{max} = 273.05\,rad/s^4$)	13.41 (Joint 4) ($S_{max} = 150\,rad/s^4$)
		1.5942	22.13 (Joint 1) ($S_{max} = 700\,rad/s^4$)	19.91 (Joint 1) ($S_{max} = 597.67\,rad/s^4$)
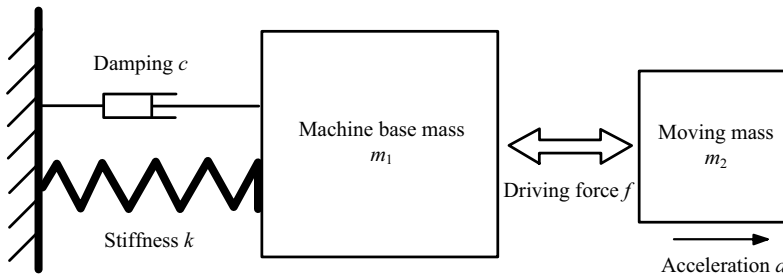
Figure 18. *A single-degree-of-freedom mass-spring-damper system.*

Or

$$\ddot{x} + 2\xi\dot{x} + \omega_n^2 x = \frac{m_2}{m_1}a \tag{35}$$

where ω_n is the angular natural frequency of the base structure, ξ is the damping ratio, and x is the vibration response of the base structure.

To carry out the simulation study, it is assumed that the ratio of the moving mass over the machine base is 0.1, the undamped natural frequency of the base is 24 Hz, with a damping ratio of 3%, that is, $m_2/m_1 = 0.1$, $\omega_n = 150.8\,rad/s$ (i.e., $f_n = 24$ Hz) and $\xi = 3\%$ [35].

For comparison, three different motion profiles are evaluated, including the locally asymmetrical profile, symmetric sigmoid S-curve profile and the proposed asymmetric sigmoid S-curve profile. The residual vibration of the base frame is then determined by considering the Eq. (35) to obtain the stage vibration. The kinematic constraints are shown in Table VII and were used in ref. [35].

We set $\alpha = 1$, $\beta = 0.265$ for the locally asymmetrical 15-segment sine jerk profile [37] and the maximum snap is set to be $5000\,m/s^4$ for the symmetric 15-segment sigmoid jerk profile [8]. We make an analysis of two cases for the proposed method, where the jerk given in Table VII is set to be the maximum allowable jerks of the acceleration stage and the maximum allowable jerks of the deceleration

Table VII. *Displacement and kinematic constraints.*

|	Displacement (m)	0.8
Kinematic constraints	Velocity (m/s)	1.24
	Acceleration (m/s^2)	6
	Jerk (m/s^3)	80
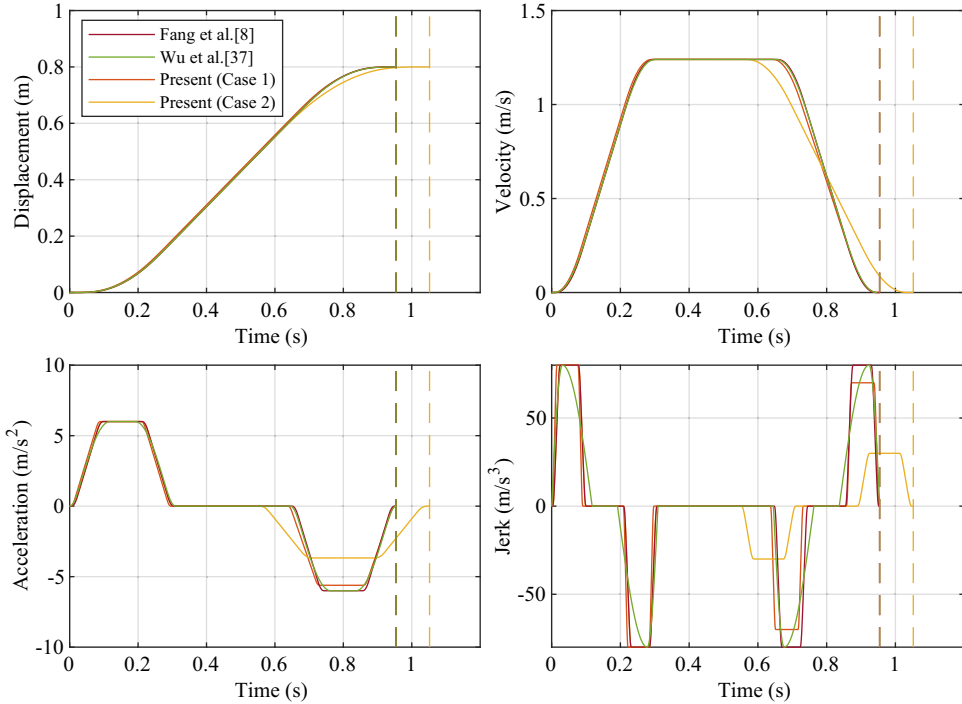
Figure 19. *Motion profiles for different trajectory models.*

stage are set to be $70 m/s^3$ and $30 m/s^3$, respectively. The maximum snaps of the acceleration stage are set to be $8000 m/s^4$ and $5000 m/s^4$. Then, the maximum snaps of the deceleration stage are obtained from Eq. (4) and Eq. (9) directly. The simulated motion profiles of the moving mass are shown in Fig. 19, and the vibrations of the base structure excited by the stage motion using the four profiles are shown in Fig. 20. As shown in Fig. 19, the total execution time for the three profiles (i.e., [8], [37] and the present method (case 1)) are all same as 0.9545s. And the execution time for the present method (case 2) is 1.0525s. Then, it is clear that the residual vibration excited by the locally asymmetrical sine jerk profile is the worst, with a peak-to-peak value of about $3 \mu m$. For the symmetric sigmoid jerk profile, the residual vibration has a peak-to-peak value of about $2.2 \mu m$, which is about 1.4 times better than the locally asymmetric profile. As shown in Fig. 20, the proposed method shows the best performance with a minimized vibration, where the residual vibration has a peak-to-peak value of about $1.9 \mu m$ for case 1 and about $0.25 \mu m$ for case 2.

As seen in the results obtained by [8] and the present (case 2), when the maximum snap of the acceleration stage is specified, the execution time is more lengthened than one of the symmetric profiles, but the generating profile is smoother and the residual vibration is smaller than one of the symmetric profiles.

The results show clearly that the performance of reducing vibrations on the machinery is good and demonstrate an important characteristic of the proposed profile suitable for high-speed point-to-point
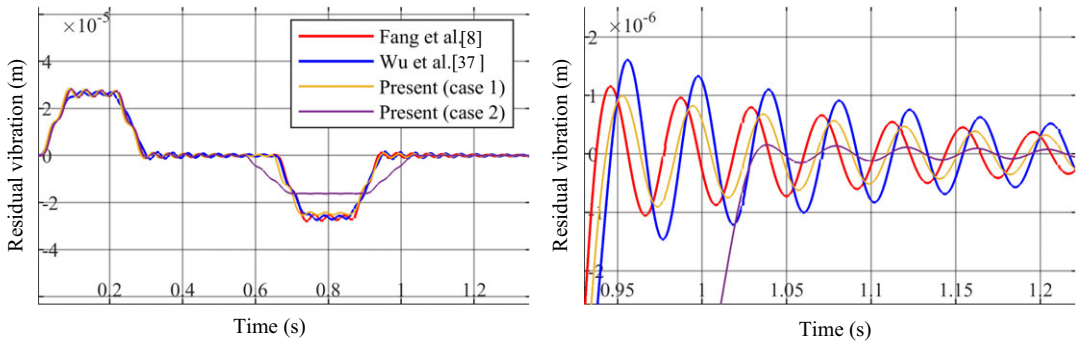
Figure 20. *Vibration response for different trajectory models.*

motion. The proposed asymmetric sigmoid profile is generated by adding one asymmetric parameter in the symmetric one presented in ref. [8], and thus, the calculation quality and time to get the optimal solution is less different for two methods. In (Fang et al. [8]), the experiments were conducted on a 6 DOF manipulator Universal Robots UR5 and the practical usability of the proposed approach was validated. The proposed method can be implemented in the same way as presented in ref. [8].

4. Conclusion

In this paper, a new method of planning asymmetric S-curve trajectories based on an expanded jerk profile is presented for smoothness and time optimality. The improved piecewise sigmoid jerk profile has been generated by introducing an asymmetric parameter. All the trajectories generated are continuous and infinitely differentiable. In addition, the values of the two end points of all derivatives are always zero. When the maximum snap of the acceleration stage is specified, the execution time is more lengthened than one of the symmetric profiles, but the generating profile is smoother and the residual vibration is smaller than one of the symmetric. However, when the maximum snap of the deceleration stage is specified, not only the smoother profile is generated but also the execution time is shorter than one of the symmetric. Thus, in the operation of assigning the smoothness of the motion, both smoothness and efficiency can be more raised. The minimum execution time has been achieved under the kinematic constraints in terms of the analytical algorithm. The results obtained through several benchmark experiments show that the proposed method can be used as the effective tool for the smooth trajectory planning of the industrial robots.

Future work will be devoted to applying the proposed method for more delicate applications requiring a complex spatial path comprising multi-points.

References

[1] S. Macfarlane and E. A. Croft, "Jerk-bounded manipulator trajectory planning: Design for real-time applications," *IEEE Trans Robot Autom* **19**(1), 42–52 (2003). doi: 10.1109/TRA.2002.807548.
[2] M.-Y. Zhao, X.-S. Gao and Q. Zhang, "An efficient stochastic approach for robust time-optimal trajectory planning of robotic manipulators under limited actuation," *Robotica* **35**(12), 2400–2417 (2017).

[3] M. D. L. Huaizhong Li, Z. M. Gong and W. Lin, "Motion profile design to reduce residual vibration of high-speed positioning stages," *IEEE/ASME Trans Mech* **14**, 264–269 (2009). doi: TMECH.2008.2012160.

[4] H. Ghariblu and M. H. Korayem, "Trajectory optimization of flexible mobile manipulators," *Robotica* **24**(3), 333–335 (2006).

[5] A. Gasparetto and V. Zanotto, "A technique for time-jerk optimal planning of robot trajectories," *Robot Com-Integr Manuf* **24**(3), 415–426 (2008). doi: 10.1016/j.rcim.2007.04.001.

[6] K. J. Kyriakopoulos and G. N. Saridis, "Minumum Jerk Path Generation," **In**: *Proceedings. 1988 IEEE International Conference on Robotics and Automation*, (1988) pp. 364–369. doi: 10.1109/ROBOT.1988.12075.

[7] V. Zanotto, A. Gasparetto, A. Lanzutti, P. Boscariol and R. Vidoni, "Experimental validation of minimum time-jerk algorithms for industrial robots," *J Intell Robotic Syst* **64**(2), 197–219 (2011).

[8] Y. Fang, J. Hu, W. Liu, Q. Shao, J. Qi and Y. Peng, "Smooth and time-optimal S-curve trajectory planning for automated robots and machines," *Mech Mach Theory* **137**, 127–153 (2019). doi: 10.1016/j.mechmachtheory.2019.03.019.

[9] M. Boryga, "The use of higher-degree polynomials for trajectory planning with jerk, acceleration and velocity constraints," *Int J Comput Appl Tech* **63**(4), 337–347 (2020). doi: 10.1504/IJCAT.2020.110414.

[10] Y. Xiao, Z. Du and W. Dong, "Smooth and near time-optimal trajectory planning of industrial robots for online applications," *Ind Robot* **39**, 169–177 (2012).

[11] R. Saravanan, S. Ramabalan and C. Balamurugan, "Multi objective trajectory planner for industrial robots with payload constraints," *Robotica* **26**(6), 753–765 (2008). doi: 10.1017/S0263574708004359.

[12] D. Zhao and H. Guo, "A trajectory planning method for polishing optical elements based on a non-uniform rational B-spline curve," *Appl Sci* **8**(8), 1355 (2018). doi: 10.3390/app8081355.

[13] J. Huang, P. Hu, K. Wu and M. Zeng, "Optimal time-jerk trajectory for industrial robots," *Mech Mach Theory* **121**, 530–544 (2018). doi: 10.1016/j.mechmachtheory.2017.11.006.

[14] H. Lie, X. Lai and W. Wu, "Time-optimal and jerk-continuous trajectory planning for robot manipulators with kinematic constraints," *Robot Com-Integr Manuf* **29**(2), 309–317 (2013). doi: 10.1016/j.rcim.2012.08.002.

[15] W. Kornmaneesang and S.-L. Chen, "Time-optimal federate scheduling with actuator constraints for 5-axis machining," *Int J Adv Manuf Technol* **119**, 6789–6807 (2022). doi: 10/21203/rs.3.rs-687810/v1.

[16] M. Boryga and A. Graboś, "Planning of manipulator motion trajectory with higher-degree polynomials use," *Mech Mach Theory* **44**(7), 1400–1419 (2009). doi: 10.1016/j.mechmachtheory.2008.11.003.

[17] S. G. Yue, D. Henrich, W. L. Xu and S. K. Tso, "Point-to-point trajectory planning of flexible redundant robot manipulators using genetic alogrithms," *Robotica* **20**(3), 269–280 (2002).

[18] H. Wang, H. Wang, J. Huang, B. Zhao and L. Quan, "Smooth point-to-point trajectory planning for industrial robots with kinematical constraints based on high-order polynomial curve," *Mech Mach Theory* **139**, 284–293 (2019). doi: 10.1016/j.mechmachtheroy.2019.05.002.

[19] D. Lee and C.-W. Ha, "Optimization process for polynomial motion profiles to achieve fast movement with low vibration," *IEEE Trans Cont Syst Technol* **28**(5), 1892–1901 (2020). doi: 10.1109/TCST.2020.2998094.

[20] L. Biagiotti and C. Melchiorri, "Optimization of generalized S-curve trajectories for residual vibration suppression and compliance with kinematic bounds," *IEEE-ASME Trans Mechatron* **26**, 2724–2734 (2021). doi: 10/1109/TMECH.2020.3045504.

[21] J. R. García-Martínez, J. Rodríguez-Reséndiz and E. E. Cruz-Miguel, "A new seven-segment profile algorithm for an open source architecture in a hybrid electronic platform," *Electronics* **8**(6), 652 (2019). doi: 10.3390/electronics8060652.

[22] H. Ni, C. Zhang, S. Ji, T. Hu, Q. Chen, Y. Liu and G. Wnag, "A bidirectional adaptive feedrate scheduling method of NURBS interpolation based on S-shaped ACC/DEC algorithm," *IEEE Access* **6**, 63794–63812 (2018).

[23] H. Mu, Y. Zhou, S. Yan and A. Han, "Third-order trajectory planning for high accuracy point-to-point motion," *Front Electric Electron Eng China* **4**(1), 83–87 (2009).

[24] T.-C. Lu and S.-L. Chen, "Shyh-leh Chen, genetic algorithm-based S-curve acceleration and deceleration for five-axis machine tools," *Int J Adv Manuf Technol* **87**(1-4), 219–232 (2016).

[25] G. Hassan, M. Gouttefarde, A. Chemori, P.-E. Herve, M. E. Rafei, C. Francis and D. Salle, "Time-optimal pick-and-throw S-curve trajectories for fast parallel robots," *IEEE/ASME Trans Mechatron* **27**(6), 4707–4717 (2022). doi: 10.1109/TMECH.2022.3164247.

[26] Y. Chen, H. Wei, K. Sun, M. Liu and T. Wang, "Algorithm for smooth S-curve feedrate profiling generation," *Chin J Mech Eng* **24**(02), 237–247 (2011). doi: 10.3901/CJME.2011.02.237.

[27] F. Song, S. Yu, T. Chen and L.-N. Sun, "Research on CNC simulation system with instruction interpretations possessed of wireless communication," *J Super-comput* **72**(7), 2703–2719 (2016).

[28] Z. M. G. Huaizhong Li and T. L. Wei Lin, "Motion profile planning for reduced jerk and vibration residuals," *SIMTech Tech Rep* **8**, 32–37 (2007). doi: 10.13140/2.1.4211.2647.

[29] Y. Fang, J. Qi, J. Hu, W. Wang and Y. Peng, "An approach for jerk-continuous trajectory generation of robotic manipulators with kinematical constraints," *Mech Mach Theory* **153**, 103957 (2020). doi: 10.1016/j.mechmachtheory.2020.103957.

[30] S. Perumaal and N. Jawahar, "Synchronized trigonometric S-curve trajectory for jerk-bounded time-optimal pick and place operation," *Int J Robot Autom* **27**(4), 385–395 (2012). doi: 10.2316/Journal.206.2012.4.206-3780.

[31] F. Zou, D. Qu, J. Wang and F. Xu, "Asymmetric Trajectory Planning for Vacuum Robot Motion," **In**: *2011 IEEE International Conference on Robotics and Automation (ICRA)*, (2011) pp. 1–4. doi: 10.1109/ICRA.2011.5980588.

[32] T. Li, Y. Liu and L. Sun, "Asymmetric velocity profile with fixed motion time for motion control," *Adv Sci Lett* **6**(1), 593–598 (2012). doi: 10.1166/ASL.2012.2200.

[33] Y. Bai, X. Chen, H. Sun and Z. Yang, "Time-optimal freeform S-curve profile under positioning error and robustness constraints," *IEEE/ASME Trans Mech* **23**, 1993–2003 (2018).

[34] X. Li, X. Gao, J. Xiao, H. Cheng, Y. Zhang and L. Hao, "Time-optimal general asymmetric S-curve profile with low residual vibration," *Mech Syst Signal Pr* **188**, 109978 (2023). doi: 10.1016/j.ymssp.2022.109978.

[35] H. Li, "A jerk-constrained asymmetric motion profile for high-speed motion stages to reduce residual vibration," *Int J Comp Appl Tech* **53**(2), 149–156 (2016). doi: 10.1504/IJCAT.2016.074453.

[36] X. Li and L. Chen, "Research on the Asymmetric S-type Curve based on the Position," **In**: *5th International Conference on Frontiers of Manufacturing Science and Measuring Technology (FMSMT 2017)*, (2017) pp. 130–1598. doi: 10.2991/fmsmt-ln.2017.310.

[37] Z. Wu, J. Chen, T. Bao, J. Wang, L. Zhang and F. Xu, "A novel point-to-point trajectory planning algorithm for industrial robots based on a locally asymmetrical jerk motion profile," *Processes* **10**(4), 728 (2022). doi: 10.3390/pr10040728.

[38] T. Liu, J. Cui, Y. Li, S. Gao, M. Zhu and L. Chen, "Time-optimal asymmetric S-curve trajectory planning of redundant manipulators under kinematic constraints," *Sensors* **23**(6), 3074 (2023). doi: 10.3390/s23063074.

[39] T. Chettibi, H. E. Lehtihet, M. Haddad and S. Hanchi, "Minimum cost trajectory planning for industrial robots," *European J Mech –A/Solids* **23**(4), 703–715 (2004). doi: 10.1016/j.euromechsol.2004.02.006.